Journal of Scientific Computing (2020) 82:9
https://doi.org/10.1007/s10915-019-01112-z

# A New Numerical Method for an Asymptotic Coupled Model of Fractured Media Aquifer System

**Wei Liu[1] · Jintao Cui[2,3] · Zhifeng Wang[4]**

Received: 8 May 2018 / Revised: 10 June 2019 / Accepted: 6 November 2019 / Published online: 8 January 2020


**Abstract**
An asymptotic model coupling three-dimensional and two-dimensional equations is considered to demonstrate the flow in fractured media aquifer system in this paper. The flow is governed by Darcy's law both in fractures and surrounding porous media. A new anisotropic and nonconforming finite element is constructed to solve the three-dimensional Darcy equation. The existence and uniqueness of the coupled solutions are deduced. Optimal error estimates are obtained in $L^2$ and $H^1$ norms. Numerical experiments show the accuracy and efficiency of the presented method. With the same number of nodal points and the same amount of computational costs, the results obtained by using the new element are much better than those by both $Q_1$ conforming element and Wilson nonconforming element on the same meshes.

**Keywords** Karst aquifers · Nonconforming finite element · Asymptotic coupled model · Numerical analysis

**Mathematics Subject Classification** 65N12 · 65N15 · 65N30

The work of Wei Liu was supported by Shandong Provincial Natural Science Foundation No. ZR2019MA049 and in part by The Hong Kong Polytechnic University AMSS-PolyU Joint Research Institute (JRI) 1-ZVA8. Jintao Cui's research is supported in part by the Hong Kong RGC, General Research Fund (GRF) Grant No. 15302518 and the National Natural Science Foundation of China (NSFC) Grant No. 11771367.

✉ Jintao Cui
jintao.cui@polyu.edu.hk

Wei Liu
sduliuwei@mail.sdu.edu.cn

Zhifeng Wang
wangzhifeng1997@163.com

1 School of Mathematics and Statistics Science, Ludong University, Yantai 264025, China

2 Department of Applied Mathematics, The Hong Kong Polytechnic University, Hung Hom, Hong Kong

3 The Hong Kong Polytechnic University Shenzhen Research Institute, Shenzhen 518057, China

4 School of Mathematics and Information Sciences, Yantai University, Yantai 264005, China

## 1 Introduction

Fracture belongs to the secondary void structure of Karst aquifer system, and occupies the major part of the total gap. It is not only the storage space of drinkable groundwater, but also the occurrence site of environmental pollution. Therefore, it is important to gain a better understanding of groundwater flow in Karst aquifer for assessing groundwater risk and controlling groundwater pollution. Flow in fractures are closely connected with that in the surrounding medium. Thus a coupled model is usually used to characterize the groundwater flow process in fractured medium, with the flux exchange occurring on the interface between the fractures and surrounding medium as the coupling term, e.g. see [1–4].

In many cases the thickness of fracture is much smaller than the characteristic diameter of the surrounding medium. So we could reduce the dimension of the flow equation for fractures and obtain an asymptotic coupled model by two approaches. One method is to employ a dirac function restricted to the fracture in the coupled term, e.g. see [5–13]. The other is to apply the averaging technique across the fracture in order to obtain the coupled term, e.g. see [14–20]. The fracture can act as a fast pathway or correspond to a geological barrier. Here we are interested in the "fast path" fracture and suppose that the pressure is continuous across the fracture, which is similar to [15,20–22]. In this paper, we consider a coupled model with different dimensions by the latter approach.

Let $\Omega_p$ be a convex domain in $\mathbb{R}^3$ with the boundary $\Gamma = \partial\Omega_p$. The fracture $\Omega_f$ is a subdomain of $\Omega_p$ and divides $\Omega_p$ into two parts, which are denoted by $\Omega_1$ and $\Omega_2$, respectively. Suppose the flow in $\Omega_1$, $\Omega_2$ and $\Omega_f$ is governed by a conservation equation together with Darcy's law as follows.

$$\begin{cases} \mathrm{div}\mathbf{u}_i = g_i & \text{in } \Omega_i, \quad i = 1, 2, f, \\ \mathbf{u}_i = -\mathbb{K}_i \nabla p_i & \text{in } \Omega_i, \quad i = 1, 2, f, \\ p_i = P_i & \text{on } \Gamma_i, \quad i = 1, 2, f, \end{cases} \tag{1.1}$$

where $\mathbf{u}$ is the Darcy velocity, $p$ is the pressure, $\mathbb{K}$ is the hydraulic conductivity(or permeability tensor), $g$ is the source or sink term, $P$ is the given pressure on the boundary. Let $p_i, \mathbf{u}_i, \mathbb{K}_i, g_i, P_i$ be the restriction of $p, \mathbf{u}, \mathbb{K}, g, P$, respectively, to $\Omega_i$, $\Gamma_i = \partial\Omega_i \cap \Gamma$ $(i = 1, 2, f)$. Here, we suppose $\mathbb{K}_i$ is diagonal and positive definite.

By using averaging across the fracture (see [14,15]), the fracture domain $\Omega_f$ is degraded to a hyperplane $\Omega_\gamma$ embedded in $\Omega_p$, see Fig. 1. Then we obtain the different dimension as 3D coupled 2D model problem.

$$\begin{cases} \mathrm{div}\mathbf{u}_i = g_i & \text{in } \Omega_i, \quad i = 1, 2, \\ \mathbf{u}_i = -\mathbb{K}_i \nabla p_i & \text{in } \Omega_i, \quad i = 1, 2, \\ \mathrm{div}_\tau \mathbf{u}_\gamma = g_\gamma + (\mathbf{u}_1 \cdot \mathbf{n}_1|_{\Omega_\gamma} + \mathbf{u}_2 \cdot \mathbf{n}_2|_{\Omega_\gamma}) & \text{in } \Omega_\gamma, \\ \mathbf{u}_\gamma = -K_{\gamma\tau} d \nabla_\tau p_\gamma & \text{in } \Omega_\gamma, \\ -\xi \mathbf{u}_i \cdot \mathbf{n}_i + \alpha_\gamma p_i = \alpha_\gamma p_\gamma - (1-\xi)\mathbf{u}_{(i+1 \bmod 2)} \cdot \mathbf{n}_{(i+1 \bmod 2)} & \text{in } \Omega_\gamma, \\ p_i = P_i & \text{on } \Gamma_i, \quad i = 1, 2, \gamma, \end{cases} \tag{1.2}$$

where $\mathbf{n}$ and $\tau$ are the tangential and normal direction to $\Omega_\gamma$. The unit vectors $\mathbf{n}_1 = -\mathbf{n}_2$ are normal to $\Omega_\gamma$. We use $\nabla_\tau$ and $\mathrm{div}_\tau$ to denote the tangential gradient and divergence. The coefficients $K_{\gamma\tau}$ and $K_{\gamma n}$ represent the equivalent permeability for the flow along and normal to the fracture, respectively. Constant $d$ is the thickness of the fracture, $\alpha_\gamma = 2K_{\gamma n}/d$ and the coefficient $\xi \in (1/2, 1]$. Here, the permeability in the fracture can be larger than that in the surrounding medium. A lager permeability fracture corresponds to a fast pathway for the fracture.

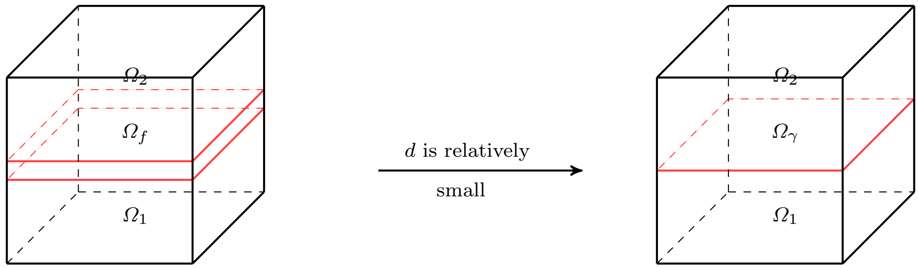


**Fig. 1** Left: the whole domain is divided by the fracture $\Omega_f$ with thickness $d$ into $\Omega_1$ and $\Omega_2$; right: $\Omega_f$ is treated as a fracture-interface $\Omega_\gamma$

Setting $\alpha = \dfrac{2\alpha_\gamma}{2\xi - 1}$, we can rewrite model (1.2) as follows,

$$\begin{cases} -\mathrm{div}(\mathbb{K}_i \nabla p_i) = g_i & \text{in } \ \Omega_i, \quad i = 1, 2, \\ -\mathrm{div}_\tau(K_{\gamma\tau} d \nabla_\tau p_\gamma) = \alpha\left(\dfrac{p_1\mid_{\Omega_\gamma} + p_2\mid_{\Omega_\gamma}}{2} - p_\gamma\right) + g_\gamma & \text{in } \ \Omega_\gamma, \\ \mathbb{K}_1 \nabla p_1 \cdot \mathbf{n}_1\mid_{\Omega_\gamma} + \mathbb{K}_2 \nabla p_2 \cdot \mathbf{n}_2\mid_{\Omega_\gamma} = \alpha\left(p_\gamma - \dfrac{p_1\mid_{\Omega_\gamma} + p_2\mid_{\Omega_\gamma}}{2}\right) & \text{in } \ \Omega_\gamma, \\ p_i = P_i & \text{on } \ \Gamma_i, \quad i = 1, 2, \gamma. \end{cases} \tag{1.3}$$

In recent years, the asymptotic model (1.2) with different dimensions has become a hot topic in studying groundwater flow process in fractured media aquifer system. Previous study mainly focused on the case where the fracture is treated as one-dimension and surrounding medium as two-dimension. Robert et al. [14,15] used $\mathrm{RT}_0$ mixed finite element method to solve the asymptotic Darcy–Darcy model and proved the existence and uniqueness of solutions. Non-overlapping domain decomposition method is applied in the numerical examples. Angot et al. [19] applied the finite volume method and proved the convergence of the numerical solutions of the asymptotic model.

In this paper, we consider the asymptotic model (1.3) with two-dimensional Darcy equation in fractures and three-dimensional Darcy equation in the surrounding media. Anisotropic and multi-scale coupling properties of the asymptotic model (1.3) perfectly match the physical characteristics of the groundwater flow problem, but bring some numerical challenges to solve it. Near the fracture hyperplane $\Omega_\gamma$, the derivative of the analytic solution along the direction perpendicular to the fracture is of a low regularity. That means that the solution of Darcy model in the porous media domain $\Omega_p$ varies significantly along the perpendicular direction to the fracture and is smooth along the direction parallel to the fracture. In order to capture significant changes near $\Omega_\gamma$, one possibility is to use anisotropic meshes which have a small mesh size near the fracture and a larger mesh size away from the fracture. Consequently, the subdivision of the anisotropic meshes depends on the position of the fracture which is unknown in many cases. To circumvent this difficulty, in this work we construct a new element with its own anisotropic property to solve the Darcy equation in porous media $\Omega_p$ without dependence on the meshes.

The new anisotropic element is motivated by $Q_1$ conforming element and Wilson nonconforming element. It is well known that the $Q_1$ element is a bilinear conforming element defined on cuboid mesh and the functions in $Q_1$ element space are continuous across every boundary surface. The Wilson element is a nonconforming element with eight conforming parts and three nonconforming parts, and the functions in Wilson nonconforming element space are discontinuous along each direction of coordinate axis (see [23–26] for details). The idea of our new element is to combine the properties and merits of $Q_1$ element and Wilson element. More precisely, the new element is constructed to be continuous (conforming) along the direction parallel to the fracture just like $Q_1$ element and discontinuous (nonconforming) along the direction perpendicular to the fracture just like Wilson element. Therefore, it can be applied appropriately to solve the partial differential equations with smooth solutions in some directions and singular solutions in other directions. The element is not conservative but it can extend to some other cases such as inclined fracture and intersecting fractures. Specially, based on Quasi-Wilson element and $Q_1$ element, the method is easily to cope with the inclined cases. The idea of construction new element can be applied to vertical intersecting fracture by using only 10 degrees of freedom on each unit. In the numerical examples, it is seen that the performance of the new nonconforming element are much better than the $Q_1$ conforming element and Wilson nonconforming element on the same mesh.

The outline of the paper is as follows. The numerical scheme combing the new nonconforming element and the conforming finite element method are presented in Sect. 2. Existence and uniqueness of approximation solution are also deduced. In Sect. 3, we give the error estimates for the approximation scheme in $L^2$ norm and $H^1$ norm. Numerical examples are presented in Sect. 4 to show the efficiency and accuracy of the new nonconforming finite element method.

## 2 A Coupled Numerical Method

The weak form for the model (1.3) is to find $\mathbf{p} = (p_1, p_2, p_\gamma) \in H_0^1(\Omega_1) \times H_0^1(\Omega_2) \times H_0^1(\Omega_\gamma)$, such that

$$\begin{cases} (\mathbb{K}_1 \nabla p_1, \nabla q_1) + (\mathbb{K}_2 \nabla p_2, \nabla q_2) - \alpha \left( p_\gamma - \dfrac{p_1 \mid_{\Omega_\gamma} + p_2 \mid_{\Omega_\gamma}}{2}, \dfrac{q_1 \mid_{\Omega_\gamma} + q_2 \mid_{\Omega_\gamma}}{2} \right) \\ \quad = (g_1, q_1) + (g_2, q_2) \qquad \forall q_1 \in H_0^1(\Omega_1), q_2 \in H_0^1(\Omega_2), \\ (K_{\gamma\tau} d \nabla_\tau p_\gamma, \nabla_\tau q_\gamma) + \alpha \left( p_\gamma - \dfrac{p_1 \mid_{\Omega_\gamma} + p_2 \mid_{\Omega_\gamma}}{2}, q_\gamma \right) = (g_\gamma, q_\gamma) \quad \forall q_\gamma \in H_0^1(\Omega_\gamma). \end{cases} \tag{2.1}$$

**Theorem 2.1** *Suppose $\mathbb{K}_1 = k_1 \mathbb{I}$ and $\mathbb{K}_2 = k_2 \mathbb{I}$, then there exists a unique solution of (2.1).*

***Proof*** In the case of homogeneous isotropic matrix, one can easily see by separation of variable that $p_1 \in H^{2+\epsilon}(\Omega_1)$ and $p_2 \in H^{2+\epsilon}(\Omega_2)$ for any $\epsilon \in (0, 1/2)$. The existence and uniqueness of solution to (2.1) are direct consequences of Lax–Milgram Theorem since the bilinear form $a(\cdot, \cdot)$ satisfies the continuity and coercivity condition on $H_0^1(\Omega_1) \times H_0^1(\Omega_2) \times H_0^1(\Omega_\gamma)$, where

$$\begin{aligned} a(\mathbf{p}, \mathbf{q}) = & \int_{\Omega_1} \mathbb{K}_1 \nabla p_1 \cdot \nabla q_1 dxdydz + \int_{\Omega_2} \mathbb{K}_2 \nabla p_2 \cdot \nabla q_2 dxdydz \\ & + \int_{\Omega_\gamma} K_{\gamma\tau} d \nabla_\tau p_\gamma \cdot \nabla_\tau q_\gamma dxdy \\ & + \alpha \int_{\Omega_\gamma} \left( p_\gamma - \frac{p_1 \mid_{\Omega_\gamma} + p_2 \mid_{\Omega_\gamma}}{2} \right) \left( q_\gamma - \frac{q_1 \mid_{\Omega_\gamma} + q_2 \mid_{\Omega_\gamma}}{2} \right) dxdy, \end{aligned} \tag{2.2}$$

$$(\mathbf{g}, \mathbf{q}) = \int_{\Omega_1} g_1 q_1 dxdydz + \int_{\Omega_2} g_2 q_2 dxdydz + \int_{\Omega_\gamma} g_\gamma q_\gamma dxdy. \tag{2.3}$$

This complete the proof. $\square$

Let $\mathcal{T}_h$ be a regular triangulation of $\Omega_p$ with a family of parallelepipeds $K_l$ $(l = 1, \ldots, N)$. Denote $h_K = \operatorname{diam}(K)$ and $h = \max_{K\in\mathcal{T}_h} h_K$. Set $\mathcal{T}_{ih} = \mathcal{T}_h|_{\Omega_i}$ with $i = 1, 2, \gamma$. For simplicity, we assume the face $\Omega_\gamma$ is perpendicular to $z$-axis. The following new element can be extended to the cases where $\Omega_\gamma$ is perpendicular to $x$-axis or $y$-axis.

The reference element is defined as $\hat{K} = [-1, 1]^3$ with eight vertices

$$\begin{aligned} &\hat{v}_1 = (-1,-1,-1),\ &&\hat{v}_2 = (-1,1,-1),\ &&\hat{v}_3 = (1,-1,-1),\\ &\hat{v}_4 = (1,1,-1), &&\hat{v}_5 = (-1,-1,1),\ &&\hat{v}_6 = (-1,1,1),\\ &\hat{v}_7 = (1,-1,1), &&\hat{v}_8 = (1,1,1). \end{aligned}$$

and

$$\hat{\mathbb{P}} = Q_1(\hat{K}) \bigoplus span\left\{\frac{(1-\hat{x}^2)(1-\hat{y}^2)}{32}\right\},$$

with

$$\widehat{\sum} = \left\{\hat{q}(\hat{v}_j),\ j = 1,\ldots,8;\ \int_{\hat{K}} \frac{\partial^4 \hat{q}}{\partial \hat{x}^2 \hat{y}^2} d\hat{x}d\hat{y}d\hat{z}\right\}.$$

Then, the basis functions of new element on the reference $\hat{K}$ are from $\hat{\mathbb{P}}$ on each unit, and the degrees of freedom are from $\widehat{\sum}$ accordingly.

Let $F_K$ be the affine mapping from $\hat{K}$ to $K$ and $J_K$ be the Jacobi matrix of $F_K$. Based on the subdivision $\mathcal{T}_h$, the nonconforming finite element space $W_{h,i}$ is defined by

$$\begin{aligned} W_{h,i} = \Big\{&w_h \in L^2(\Omega_i) : w_h|_K = \hat{w}_h(\hat{x}, \hat{y}, \hat{z}) \circ F_K^{-1},\ \forall \hat{w}_h \in \hat{\mathbb{P}} \text{ and } K \in \mathcal{T}_{ih} (i = 1, 2);\\ &w_h = 0 \text{ at the vertices belonging to } \partial\Omega_i\}. \end{aligned}$$

Let $W_{h,\gamma} \subset H_0^1(\Omega_\gamma)$ be the continuous piecewise linear polynomial space with respect to $\mathcal{T}_{\gamma h}$. A coupled scheme based on finite element approximation scheme for (2.1) is to find $\mathbf{p}_h = (p_{1h}, p_{2h}, p_{\gamma h}) \in W_{h,1} \times W_{h,2} \times W_{h,\gamma}$ satisfying that

$$a_h(\mathbf{p}_h, \mathbf{q}_h) = (\mathbf{g}, \mathbf{q}_h), \quad \forall\ \mathbf{q}_h = (q_{1h}, q_{2h}, q_{\gamma h}) \in W_{h,1} \times W_{h,2} \times W_{h,\gamma}. \tag{2.4}$$

where

$$\begin{aligned} &a_h(\mathbf{p}_h, \mathbf{q}_h)\\ &= \sum_{K\in\mathcal{T}_{1h}} \int_K \mathbb{K}_1 \nabla p_{1h} \cdot \nabla q_{1h} dxdydz + \sum_{K\in\mathcal{T}_{2h}} \int_K \mathbb{K}_2 \nabla p_{2h} \cdot \nabla q_{2h} dxdydz\\ &\quad + \sum_{E\in\mathcal{T}_{\gamma h}} \int_E K_{\gamma\tau} d \nabla_\tau p_{\gamma h} \cdot \nabla_\tau q_{\gamma h} dxdy\\ &\quad + \alpha \sum_{E\in\mathcal{T}_{\gamma h}} \int_E \left(p_{\gamma h} - \frac{p_{1h}\,|_{\Omega_\gamma} + p_{2h}\,|_{\Omega_\gamma}}{2}\right)\left(q_{\gamma h} - \frac{q_{1h}\,|_{\Omega_\gamma} + q_{2h}\,|_{\Omega_\gamma}}{2}\right) dxdy. \end{aligned} \tag{2.5}$$

For any $\mathbf{p}_h = (p_{1h}, p_{2h}, p_{\gamma h}) \in W_{h,1} \times W_{h,2} \times W_{h,\gamma}$, we introduce the norm

$$\|\mathbf{p}_h\|_{1,h} = \left(\sum_{K\in\mathcal{T}_{1h}} |p_{1h}|_{1,K}^2\right)^{1/2} + \left(\sum_{K\in\mathcal{T}_{2h}} |p_{2h}|_{1,K}^2\right)^{1/2} + \|p_{\gamma h}\|_{1,\Omega_\gamma}. \tag{2.6}$$

**Lemma 2.1** *Suppose $\hat{q} \in \hat{\mathbb{P}}$ vanishes at the eight vertices $\hat{v}_j$ $(j = 1, \ldots, 8)$ and the integral value defined as in $\widehat{\sum}$, then $\hat{q} \equiv 0$.*

From the above lemma, we can define the new element $(\hat{K}, \hat{\mathbb{P}}, \widehat{\sum})$ over $\hat{K}$ with nine degrees of freedom such that

(1) $\hat{K}$ is the reference cube,
(2) $\hat{\mathbb{P}}$ is the shape function space,
(3) $\widehat{\sum}$ is the set of degrees of freedom.

**Lemma 2.2** *The functions in $W_{h,i}$ $(i = 1, 2)$ are continuous along both $x$-direction and $y$-direction, but discontinuous along the $z$-direction.*

***Proof*** By Lemma 2.2, $\hat{q}$ is uniquely determined by

$$\hat{q}(\hat{x}, \hat{y}, \hat{z}) = \sum_{j=1}^{8} \hat{q}(\hat{v}_j)\hat{N}_j(\hat{x}, \hat{y}, \hat{z}) + \hat{N}_9(\hat{x}, \hat{y}, \hat{z}) \int_{\hat{K}} \frac{\partial^4 \hat{q}}{\partial \hat{x}^2 \hat{y}^2} d\hat{x} d\hat{y} d\hat{z},$$

where $\hat{N}_j(\hat{x}, \hat{y}, \hat{z}) \in Q_1(\hat{K})$ (for $j = 1, \ldots, 8$) and $\hat{N}_9 = \dfrac{(1-\hat{x}^2)(1-\hat{y}^2)}{32}$.

For any $q_h \in W_{h,p}$, we denote

$$\begin{aligned} q_h|_K &= \hat{q}_h|_{\hat{K}} \circ F_K^{-1} \\ &= \left( \sum_{j=1}^{8} \hat{q}_h(\hat{v}_j)\hat{N}_j(\hat{x}, \hat{y}, \hat{z}) \right) \circ F_K^{-1} + \left( \hat{N}_9(\hat{x}, \hat{y}, \hat{z}) \int_{\hat{K}} \frac{\partial^4 \hat{q}_h}{\partial \hat{x}^2 \hat{y}^2} d\hat{x} d\hat{y} d\hat{z} \right) \circ F_K^{-1} \\ &:= \overline{q_h} + \widetilde{q_h}. \end{aligned} \tag{2.7}$$

Same as the functions in $Q_1$ finite element, $\overline{q_h}$ is continuous across each boundary face of the brick element and is called the conforming part of the new nonconforming finite element. The other part $\widetilde{q_h}$ is the nonconforming one of the new nonconforming finite element. It is easy to check $\widetilde{q_h}$ is continuous along the $x$-direction and $y$-direction. However, this part is discontinuous along the $z$-direction across the brick element boundary face. Therefore, any element $q_h \in W_{h,i}$ $(i = 1, 2)$ are continuous along the $x$-direction and $y$-direction but discontinuous along the $z$-direction. □

**Lemma 2.3** *For any $q_h \in W_{h,i}$ and $K \in \mathcal{T}_{ih} (i = 1, 2)$, there exists a positive constant $C$ such that*

$$|\widetilde{q_h}|_{1,K} \le C|q_h|_{1,K}, \tag{2.8}$$

$$|\overline{q_h}|_{1,K} \le C|q_h|_{1,K}, \tag{2.9}$$

$$\|\widetilde{q_h}\|_{0,\partial K} \le C h_K^{1/2} |\widetilde{q_h}|_{1,K}, \tag{2.10}$$

*where $\widetilde{q_h}$ and $\overline{q_h}$ are the nonconforming part and conforming part of $q_h$, respectively.*

***Proof*** Using the parity of integrable functions and the definition (2.7),

$$\int_{\hat{K}} \frac{\partial \widehat{\widetilde{q_h}}}{\partial \hat{x}} \frac{\partial \widehat{\overline{q_h}}}{\partial \hat{x}} d\hat{x} d\hat{y} d\hat{z} = \int_{\hat{K}} \frac{\partial \widehat{\widetilde{q_h}}}{\partial \hat{y}} \frac{\partial \widehat{\overline{q_h}}}{\partial \hat{y}} d\hat{x} d\hat{y} d\hat{z} = 0.$$

Due to the fact that $\widehat{\widetilde{q_h}}$ has nothing to do with $\hat{z}$, we have

$$\int_{\hat{K}} \frac{\partial \widehat{\widetilde{q_h}}}{\partial \hat{z}} \frac{\partial \widehat{\overline{q_h}}}{\partial \hat{z}} d\hat{x} d\hat{y} d\hat{z} = 0.$$

Therefore, the conforming and nonconforming parts are orthogonal. Hence we can get the following equation,

$$
\begin{aligned}
|\hat{q}_h|^2_{1,\hat{K}} &= \int_{\hat{K}} \left( \left( \frac{\partial \widehat{\widehat{q_h}}}{\partial \hat{x}} + \frac{\partial \widehat{\overline{q_h}}}{\partial \hat{x}} \right)^2 + \left( \frac{\partial \widehat{\widehat{q_h}}}{\partial \hat{y}} + \frac{\partial \widehat{\overline{q_h}}}{\partial \hat{y}} \right)^2 + \left( \frac{\partial \widehat{\widehat{q_h}}}{\partial \hat{z}} + \frac{\partial \widehat{\overline{q_h}}}{\partial \hat{z}} \right)^2 \right) d\hat{x}d\hat{y}d\hat{z} \\
&= |\widehat{\widehat{q_h}}|^2_{1,\hat{K}} + |\widehat{\overline{q_h}}|^2_{1,\hat{K}}.
\end{aligned} \tag{2.11}
$$

By the regularity of mesh and the property of affine transforming and (2.11), we get

$$
\begin{aligned}
|\widetilde{q_h}|^2_{1,K} = \int_{\hat{K}} &\left( \left( \frac{\partial \widehat{\widetilde{q_h}}}{\partial \hat{x}} \frac{\partial \hat{x}}{\partial x} + \frac{\partial \widehat{\widetilde{q_h}}}{\partial \hat{y}} \frac{\partial \hat{y}}{\partial x} + \frac{\partial \widehat{\widetilde{q_h}}}{\partial \hat{z}} \frac{\partial \hat{x}}{\partial x} \right)^2 \right. \\
&+ \left( \frac{\partial \widehat{\widetilde{q_h}}}{\partial \hat{x}} \frac{\partial \hat{x}}{\partial y} + \frac{\partial \widehat{\widetilde{q_h}}}{\partial \hat{y}} \frac{\partial \hat{y}}{\partial y} + \frac{\partial \widehat{\widetilde{q_h}}}{\partial \hat{z}} \frac{\partial \hat{y}}{\partial y} \right)^2 \\
&+ \left. \left( \frac{\partial \widehat{\widetilde{q_h}}}{\partial \hat{x}} \frac{\partial \hat{x}}{\partial z} + \frac{\partial \widehat{\widetilde{q_h}}}{\partial \hat{y}} \frac{\partial \hat{y}}{\partial z} + \frac{\partial \widehat{\widetilde{q_h}}}{\partial \hat{z}} \frac{\partial \hat{z}}{\partial y} \right)^2 \right) |J_K| d\hat{x}d\hat{y}d\hat{z} \\
\leq C&|q_h|^2_{1,K}.
\end{aligned} \tag{2.12}
$$

Using the same techniques as in (2.12), we have

$$
|\overline{q_h}|_{1,K} \leq C|q_h|_{1,K}.
$$

From the definition of $\widehat{\widetilde{q_h}}$ and simple computation, we see that

$$
\|\widehat{\widetilde{q_h}}\|^2_{0,\hat{K}} = \frac{1}{450} \left( \int_{\hat{K}} \frac{\partial^4 \hat{q}_h}{\partial \hat{x}^2 \hat{y}^2} d\hat{x}d\hat{y}d\hat{z} \right)^2, \tag{2.13}
$$

$$
|\widehat{\widetilde{q_h}}|^2_{1,\hat{K}} = \frac{1}{90} \left( \int_{\hat{K}} \frac{\partial^4 \hat{q}_h}{\partial \hat{x}^2 \hat{y}^2} d\hat{x}d\hat{y}d\hat{z} \right)^2. \tag{2.14}
$$

It follows from affine transforming and (2.13) that

$$
\begin{aligned}
\sum_{E \in \partial K} \int_E \widetilde{q_h}^2 ds &\leq C h_K^2 \int_{-1}^{1} \int_{-1}^{1} (\widehat{\widetilde{q_h}}(\hat{x}, \hat{y}, -1) + \widehat{\widetilde{q_h}}(\hat{x}, \hat{y}, 1))^2 d\hat{x}d\hat{y} \\
&\leq C \frac{h_K^2}{450} \left( \int_{\hat{K}} \frac{\partial^4 \hat{q}_h}{\partial \hat{x}^2 \hat{y}^2} d\hat{x}d\hat{y}d\hat{z} \right)^2 \\
&\leq C h_K |\widetilde{q_h}|^2_{1,K}.
\end{aligned} \tag{2.15}
$$

□

**Theorem 2.2** *There exists a unique solution* $\mathbf{p}_h = (p_{1h}, p_{2h}, p_{\gamma h}) \in W_{h,1} \times W_{h,2} \times W_{h,\gamma}$ *satisfying the approximation scheme* (2.4).

***Proof*** Since the finite element subspaces $W_{h,\gamma} \subset H_0^1(\Omega_\gamma)$ consists of continuous piecewise polynomials, we have $p_{\gamma h} \subset H_0^1(\Omega_\gamma)$. Then by using the assumptions on hydraulic conductivity tensor $\mathbb{K}_1, \mathbb{K}_2$ and the constant $K_{\gamma\tau}$, we get that for any a $\mathbf{p}_h = (p_{1h}, p_{2h}, p_{\gamma h}) \in W_{h,1} \times W_{h,2} \times W_{h,\gamma}$,

$$
\begin{aligned}
a_h(\mathbf{p}_h, \mathbf{p}_h) = & \sum_{K \in \mathcal{T}_{1h}} \int_K \mathbb{K}_1 \nabla p_{1h} \cdot \nabla p_{1h} dxdydz + \sum_{K \in \mathcal{T}_{2h}} \int_K \mathbb{K}_2 \nabla p_{2h} \cdot \nabla p_{2h} dxdydz \\
& + \sum_{E \in \mathcal{T}_{\gamma h}} \int_E K_{\gamma\tau} d \nabla_\tau p_{\gamma h} \cdot \nabla_\tau p_{\gamma h} dxdy \\
& + \alpha \sum_{E \in \mathcal{T}_{\gamma h}} \int_E \left( p_{\gamma h} - \frac{p_{1h} \mid_{\Omega_\gamma} + p_{2h} \mid_{\Omega_\gamma}}{2} \right) \left( p_{\gamma h} - \frac{p_{1h} \mid_{\Omega_\gamma} + p_{2h} \mid_{\Omega_\gamma}}{2} \right) dxdy \\
& \geq C \left( \sum_{K \in \mathcal{T}_{1h}} |p_{1h}|_{1,K}^2 + \sum_{K \in \mathcal{T}_{2h}} |p_{2h}|_{1,K}^2 + \|p_{\gamma h}\|_{1,\Omega_\gamma}^2 \right) \\
& \geq C \left( \left( \sum_{K \in \mathcal{T}_{1h}} |p_{1h}|_{1,K}^2 \right)^{1/2} + \left( \sum_{K \in \mathcal{T}_{2h}} |p_{2h}|_{1,K}^2 \right)^{1/2} + \|p_{\gamma h}\|_{1,\Omega_\gamma} \right)^2 .
\end{aligned} \tag{2.16}
$$

Therefore, the approximation bilinear form (2.5) is uniformly elliptic in space $W_{h,1} \times W_{h,2} \times W_{h,\gamma}$.

By using Lemma 2.2, Lemma 2.3 and trace theorem for the conforming part $\overline{p_{ih}}$, we get for $i = 1, 2$,

$$
\begin{aligned}
\sum_{E \in \partial K} \int_E p_{ih}^2 ds & \leq \frac{1}{2} \sum_{E \in \partial K} \int_E (\widetilde{p_{ih}}^2 + \overline{p_{ih}}^2) ds \\
& \leq C \left( h_K |\widetilde{p_{ih}}|_{1,K}^2 + \sum_{E \in \partial K} \int_E \overline{p_{ih}}^2 ds \right) \leq C |p_{ih}|_{1,K}.
\end{aligned} \tag{2.17}
$$

Therefore, for any $\mathbf{q}_h = (q_{1h}, q_{2h}, q_{\gamma h}) \in W_{h,1} \times W_{h,2} \times W_{h,\gamma}$, it follows from (2.5), (2.6), Hölder inequality and trace theorem for the conforming parts that

$$
\begin{aligned}
& a_h(\mathbf{p}_h, \mathbf{q}_h) \\
& = \sum_{K \in \mathcal{T}_{1h}} \int_K \mathbb{K}_1 \nabla p_{1h} \cdot \nabla q_{1h} dxdydz + \sum_{K \in \mathcal{T}_{2h}} \int_K \mathbb{K}_2 \nabla p_{2h} \cdot \nabla q_{2h} dxdydz \\
& \quad + \sum_{E \in \mathcal{T}_{\gamma h}} \int_E K_{\gamma\tau} d \nabla_\tau p_{\gamma h} \cdot \nabla_\tau q_{\gamma h} dxdy \\
& \quad + \alpha \sum_{E \in \mathcal{T}_{\gamma h}} \int_E \left( p_{\gamma h} - \frac{p_{1h} \mid_{\Omega_\gamma} + p_{2h} \mid_{\Omega_\gamma}}{2} \right) \left( q_{\gamma h} - \frac{q_{1h} \mid_{\Omega_\gamma} + q_{2h} \mid_{\Omega_\gamma}}{2} \right) dxdy \\
& \leq C \left( \left( \sum_{K \in \mathcal{T}_{1h}} |p_{1h}|_{1,K}^2 \right)^{1/2} \left( \sum_{K \in \mathcal{T}_{1h}} |q_{1h}|_{1,K}^2 \right)^{1/2} + \left( \sum_{K \in \mathcal{T}_{2h}} |p_{2h}|_{1,K}^2 \right)^{1/2} \left( \sum_{K \in \mathcal{T}_{2h}} |q_{2h}|_{1,K}^2 \right)^{1/2} \right. \\
& \quad + \|p_{\gamma h}\|_{1,\Omega_\gamma} \|q_{\gamma h}\|_{1,\Omega_\gamma} + \left( \sum_{K \in \mathcal{T}_{1h}} |p_{1h}|_{1,K}^2 \right)^{1/2} \|q_{\gamma h}\|_{1,\Omega_\gamma} \\
& \quad + \left( \sum_{K \in \mathcal{T}_{2h}} |p_{2h}|_{1,K}^2 \right)^{1/2} \|q_{\gamma h}\|_{1,\Omega_\gamma} \\
& \quad \left. + \|p_{\gamma h}\|_{1,\Omega_\gamma} \left( \sum_{K \in \mathcal{T}_{1h}} |q_{1h}|_{1,K}^2 \right)^{1/2} + \|p_{\gamma h}\|_{1,\Omega_\gamma} \left( \sum_{K \in \mathcal{T}_{2h}} |q_{2h}|_{1,K}^2 \right)^{1/2} \right)
\end{aligned}
$$

$$
\begin{aligned}
&\leq C\left(\left(\sum_{K\in\mathcal{T}_{1h}}|p_{1h}|_{1,K}^2\right)^{1/2}+\left(\sum_{K\in\mathcal{T}_{2h}}|p_{2h}|_{1,K}^2\right)^{1/2}+\|p_{\gamma h}\|_{1,\Omega_\gamma}\right)\\
&\quad\times\left(\left(\sum_{K\in\mathcal{T}_{1h}}|q_{1h}|_{1,K}^2\right)^{1/2}+\left(\sum_{K\in\mathcal{T}_{2h}}|q_{2h}|_{1,K}^2\right)^{1/2}+\|q_{\gamma h}\|_{1,\Omega_\gamma}\right)\\
&= C_2\|\mathbf{p}_h\|_{1,h}\|\mathbf{q}_h\|_{1,h}. \qquad (2.18)
\end{aligned}
$$

By the Lax–Milgram Theorem, there exists a unique solution $\mathbf{p}_h \in W_{h,1}\times W_{h,2}\times W_{h,\gamma}$ of (2.4). □

## 3 Error Estimates

First, we introduce some interpolation operators for the new nonconforming element on the domain $\Omega_i$ $(i = 1, 2)$ as follows. On the reference element $\hat{K}$, denote the interpolation operator $\hat{\Pi}_K : H^2(\hat{K}) \to P_2(\hat{K})$ by

$$
\hat{\Pi}_K\hat{q} = \sum_{j=1}^{8}\hat{N}_j(\hat{x},\hat{y},\hat{z})\hat{q}(\hat{v}_j). \qquad (3.1)
$$

On the physical element $K$, the interpolation operators are defined as

$$
\Pi_K : H^2(K) \to P_2(K) \quad \text{with} \quad \Pi_K q = (\hat{\Pi}_K\hat{q})\circ F_K^{-1}.
$$

Then we define

$$
\Pi_i : H^2(\Omega_i) \to q_h, \quad \text{and} \quad \Pi_i|_K = \Pi_K, \quad \text{with } i = 1, 2. \qquad (3.2)
$$

Due to the interpolation property, we have that

$$
|q_i - \Pi_i q_i|_{k,h} \leq Ch^{l-k}|q_i|_{l,h}, \qquad 0\leq k\leq l\leq 2,\ i = 1, 2. \qquad (3.3)
$$

For the fracture domain $\Omega_\gamma$, the continuous piecewise linear interpolation operator $\Pi_\gamma$ : $H^2(\Omega_\gamma) \to W_{h,\gamma}$ has the property that

$$
\|q_\gamma - \Pi_\gamma q_\gamma\|_{1,\Omega_\gamma} \leq Ch\|q_\gamma\|_{2,\Omega_\gamma}. \qquad (3.4)
$$

**Lemma 3.1** *Assume* $\mathbf{p} = (p_1, p_2, p_\gamma)$ *and* $\mathbf{p}_h = (p_{1h}, p_{2h}, p_{\gamma h})$ *be defined by* (2.1) *and* (2.4)*, respectively, we have the following error estimate*

$$
\begin{aligned}
\|\mathbf{p}-\mathbf{p}_h\|_{1,h} \leq C\Bigg(&\inf_{\mathbf{q}_h\in W_{h,1}\times W_{h,2}\times W_{h,\gamma}}\|\mathbf{p}-\mathbf{q}_h\|_{1,h}\\
&+\sup_{\mathbf{v}_h\in(W_{h,1}\times W_{h,2}\times W_{h,\gamma})\backslash\{\mathbf{0}\}}\frac{|E_h(\mathbf{p},\mathbf{v}_h)|}{\|\mathbf{v}_h\|_{1,h}}\Bigg), \qquad (3.5)
\end{aligned}
$$

*where* $\mathbf{v}_h = (v_{1h}, v_{2h}, v_{\gamma h})$ *and*

$$E_h(\mathbf{p}, \mathbf{v}_h) = \sum_{K \in \mathcal{T}_{1h}} \int_{\partial K} \mathbb{K}_1 \nabla p_1 \cdot \nu_1 \widetilde{v_{1h}} ds + \sum_{K \in \mathcal{T}_{2h}} \int_{\partial K} \mathbb{K}_2 \nabla p_2 \cdot \nu_2 \widetilde{v_{2h}} ds - \alpha \sum_{E \in \mathcal{T}_{\gamma h}} \int_E \left( p_\gamma - \frac{p_1 \mid_{\Omega_\gamma} + p_2 \mid_{\Omega_\gamma}}{2} \right) \left( \frac{\widetilde{v_{1h}} \mid_{\Omega_\gamma} + \widetilde{v_{2h}} \mid_{\Omega_\gamma}}{2} \right) dxdy, \tag{3.6}$$

*and $\nu_i$ is the unit outer normal vector of $\partial K_i$ for $K_i \in \mathcal{T}_{ih}$ with $i = 1, 2$.*

***Proof*** Combining (2.1) and the nonconforming element scheme (2.4), we have

$$\begin{aligned} a_h(\mathbf{p} - \mathbf{p}_h, \mathbf{q}_h) &= a_h(\mathbf{p}, \mathbf{q}_h) - (\mathbf{g}, \mathbf{q}_h) \\ &= \sum_{K \in \mathcal{T}_{1h}} \int_{\partial K} \mathbb{K}_1 \nabla p_1 \cdot \nu_1 \widetilde{q_{1h}}\, ds + \sum_{K \in \mathcal{T}_{2h}} \int_{\partial K} \mathbb{K}_2 \nabla p_2 \cdot \nu_2 \widetilde{q_{2h}}\, ds \\ &\quad + \alpha \sum_{E \in \mathcal{T}_{\gamma h}} \int_E \left( p_\gamma - \frac{p_1 \mid_{\Omega_\gamma} + p_2 \mid_{\Omega_\gamma}}{2} \right) \left( \frac{\widetilde{q_{1h}} \mid_{\Omega_\gamma} + \widetilde{q_{2h}} \mid_{\Omega_\gamma}}{2} \right) dxdy \\ &:= E_h(\mathbf{p}, \mathbf{q}_h). \end{aligned} \tag{3.7}$$

According to the continuity and coercivity of of $a_h(\cdot, \cdot)$ and (3.7), we have that

$$\|\mathbf{q}_h - \mathbf{p}_h\|_{1,h}^2 \leq C \|\mathbf{p} - \mathbf{q}_h\|_{1,h} \|\mathbf{q}_h - \mathbf{p}_h\|_{1,h} + E_h(\mathbf{p}, \mathbf{q}_h - \mathbf{p}_h). \tag{3.8}$$

Hence we get

$$\|\mathbf{q}_h - \mathbf{p}_h\|_{1,h} \leq C \left( \|\mathbf{p} - \mathbf{v}_h\|_{1,h} + \sup_{\substack{\mathbf{v}_h = (v_{1h}, v_{2h}, v_{\gamma h}) \\ \in (W_{h,1} \times W_{h,2} \times W_{h,\gamma}) \setminus \{\mathbf{0}\}}} \frac{|E_h(\mathbf{p}, \mathbf{v}_h)|}{\|\mathbf{v}_h\|_{1,h}} \right). \tag{3.9}$$

Finally, we can obtain (3.5) directly by using triangular inequality. □

**Lemma 3.2** *For any $q_h \in W_{h,i}$ $(i = 1, 2)$, we have*

$$\|\widetilde{q_h}\|_{0,K} \leq Ch|q_h|_{1,K}. \tag{3.10}$$

***Proof*** It directly follows from the affine transformation (2.11) and (2.13) that

$$\begin{aligned} \|\widetilde{q_h}\|_{0,K}^2 &\leq Ch_K^3 \|\widehat{\widetilde{q_h}}\|_{0,\hat{K}}^2 \\ &\leq Ch_K^3 |\widehat{\widetilde{q_h}}|_{1,\hat{K}}^2 \\ &\leq Ch_K^3 |\widehat{q_h}|_{1,\hat{K}}^2 \\ &\leq Ch^2 |q_h|_{1,K}^2. \end{aligned} \tag{3.11}$$

□

Note that $\widetilde{q_h}$ is not a constant function due to the fact that it has nonconforming and discontinuous properties.

**Theorem 3.1** *Let $\mathbb{K}_1 = k_1 \mathbb{I}$, $\mathbb{K}_2 = k_2 \mathbb{I}$, $\mathbf{p} = (p_1, p_2, p_\gamma)$ and $\mathbf{p}_h = (p_{1h}, p_{2h}, p_{\gamma h})$ be defined by* (2.1) *and* (2.4)*, respectively, then we get*

$$\|\mathbf{p} - \mathbf{p}_h\|_{1,h} \leq Ch \left( |p_1|_{2,h} + |p_2|_{2,h} + \|p_\gamma\|_{2,\Omega_\gamma} \right), \tag{3.12}$$

*where the constant $C$ depends on the hydraulic conductivity tensors $\mathbb{K}_1, \mathbb{K}_2$, the conduct constant $\mathbb{K}_{\gamma\tau}$, the pressures $p_1, p_2, p_\gamma$ and the subdivision of mesh grids.*

**Fig. 2** Unit $K$

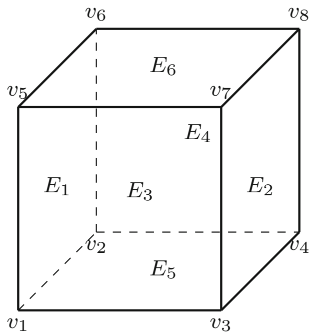


***Proof*** By Lemma 3.1, we will need to estimate the two terms on the right hand of (3.5). For the first term which corresponds to the interpolation error, we can applied (3.3) and (3.4) to get

$$\begin{aligned}
&\inf_{\mathbf{p}_h\in W_{h,1}\times W_{h,2}\times W_{h,\gamma}} \|\mathbf{p}-\mathbf{p}_h\|_{1,h} \\
&\quad\le |p_1-\Pi_1 p_1|_{1,h}+|p_2-\Pi_2 p_2|_{1,h}+\|p_\gamma-\Pi_\gamma p_\gamma\|_{1,\Omega_\gamma} \\
&\quad\le Ch\left(\sum_{K\in\mathcal{T}_{1h}}|p_1|_{2,K}+\sum_{K\in\mathcal{T}_{2h}}|p_2|_{2,K}+\|p_\gamma\|_{2,\Omega_\gamma}\right). \qquad (3.13)
\end{aligned}$$

Let $\nu_1=(\nu_{11},\nu_{12},\nu_{13})$ and $\nu_2=(\nu_{21},\nu_{22},\nu_{23})$ be the unit outer normal vectors to the faces of physical element $K$,

According to the definition of $\widetilde{q_{1h}}$ and Fig. 2, we see that $\widetilde{q_{1h}}|_{E_1}=\widetilde{q_{1h}}|_{E_2}=\widetilde{q_{1h}}|_{E_3}=\widetilde{q_{1h}}|_{E_4}=0$ and $\widetilde{q_{1h}}|_{E_5}=\widetilde{q_{1h}}|_{E_6}$. Therefore,

$$\int_{\partial K}\widetilde{q_{1h}}\nu_{11}=\int_{\partial K}\widetilde{q_{1h}}\nu_{12}=\int_{\partial K}\widetilde{q_{1h}}\nu_{13}=0. \qquad (3.14)$$

Similarly,

$$\int_{\partial K}\widetilde{q_{2h}}\nu_{21}=\int_{\partial K}\widetilde{q_{2h}}\nu_{22}=\int_{\partial K}\widetilde{q_{2h}}\nu_{23}=0. \qquad (3.15)$$

For the second term on the right-hand side of (3.5), we apply Lemma 2.3, Lemma 3.2, (3.14), (3.15) to obtain that

$$\begin{aligned}
&|E_h(\mathbf{p},\mathbf{q}_h)| \\
&=\Bigg|\sum_{K\in\mathcal{T}_{1h}}\int_{\partial K}\mathbb{K}_1\nabla p_1\cdot\nu_1\widetilde{q_{1h}}ds+\sum_{K\in\mathcal{T}_{2h}}\int_{\partial K}\mathbb{K}_2\nabla p_2\cdot\nu_2\widetilde{q_{2h}}ds \\
&\quad-\alpha\sum_{E\in\mathcal{T}_{\gamma h}}\int_E\left(p_\gamma-\frac{p_1\,|_{\Omega_\gamma}+p_2\,|_{\Omega_\gamma}}{2}\right)\left(\frac{\widetilde{q_{1h}}\,|_{\Omega_\gamma}+\widetilde{q_{2h}}\,|_{\Omega_\gamma}}{2}\right)dxdy\Bigg| \\
&=\Bigg|\sum_{E\in\mathcal{T}_{\gamma h}}\int_E\mathbb{K}_1\nabla p_1\cdot\nu_1\widetilde{q_{1h}}ds+\sum_{E\in\mathcal{T}_{\gamma h}}\int_E\mathbb{K}_2\nabla p_2\cdot\nu_2\widetilde{q_{2h}}ds
\end{aligned}$$

$$
\begin{aligned}
&-\alpha \sum_{E\in\mathcal{T}_{\gamma h}} \int_E \left(p_\gamma - \frac{p_1\mid_{\Omega_\gamma} + p_2\mid_{\Omega_\gamma}}{2}\right)\left(\frac{\widetilde{q_{1h}}\mid_{\Omega_\gamma} + \widetilde{q_{2h}}\mid_{\Omega_\gamma}}{2}\right) dxdy \\
&+ \left.\sum_{E\in\partial\mathcal{T}_{1h}\backslash\mathcal{T}_{\gamma h}} \int_E \mathbb{K}_1\nabla p_1\cdot\nu_1\widetilde{q_{1h}}ds + \sum_{E\in\partial\mathcal{T}_{2h}\backslash\mathcal{T}_{\gamma h}} \int_E \mathbb{K}_2\nabla p_2\cdot\nu_2\widetilde{q_{2h}}ds\right| \\
&= \left|\sum_{E\in\partial\mathcal{T}_{1h}\backslash\mathcal{T}_{\gamma h}} \int_E \mathbb{K}_1\nabla p_1\cdot\nu_1\widetilde{q_{1h}}ds + \sum_{E\in\partial\mathcal{T}_{2h}\backslash\mathcal{T}_{\gamma h}} \int_E \mathbb{K}_2\nabla p_2\cdot\nu_2\widetilde{q_{2h}}ds\right| \\
&\le C\left(\left|\sum_{E\in\partial\mathcal{T}_{1h}\backslash\mathcal{T}_{\gamma h}} \int_E \left(\frac{\partial p_1}{\partial x}\nu_{11}\widetilde{q_{1h}} + \frac{\partial p_1}{\partial y}\nu_{12}\widetilde{q_{1h}} + \frac{\partial p_1}{\partial z}\nu_{13}\widetilde{q_{1h}}\right)ds\right|\right. \\
&\left.+ \left|\sum_{E\in\partial\mathcal{T}_{2h}\backslash\mathcal{T}_{\gamma h}} \int_E \left(\frac{\partial p_2}{\partial x}\nu_{21}\widetilde{q_{2h}} + \frac{\partial p_2}{\partial y}\nu_{22}\widetilde{q_{2h}} + \frac{\partial p_2}{\partial z}\nu_{23}\widetilde{q_{2h}}\right)ds\right|\right) \\
&= C\left(\left|\sum_{E\in\partial\mathcal{T}_{1h}\backslash\mathcal{T}_{\gamma h}} \int_E \left(\left(\frac{\partial p_1}{\partial x} - M_1\left(\frac{\partial p_1}{\partial x}\right)\right)\widetilde{q_{1h}}\nu_{11} + \left(\frac{\partial p_1}{\partial y} - M_1\left(\frac{\partial p_1}{\partial y}\right)\right)\widetilde{q_{1h}}\nu_{12}\right.\right.\right. \\
&\left.\left.+ \left(\frac{\partial p_1}{\partial z} - M_1\left(\frac{\partial p_1}{\partial z}\right)\right)\widetilde{q_{1h}}\nu_{13}\right)ds\right| + \left|\sum_{E\in\partial\mathcal{T}_{2h}\backslash\mathcal{T}_{\gamma h}} \int_E \left(\left(\frac{\partial p_2}{\partial x} - M_2\left(\frac{\partial p_2}{\partial x}\right)\right)\widetilde{q_{2h}}\nu_{21}\right.\right. \\
&\left.\left.\left.+ \left(\frac{\partial p_2}{\partial y} - M_2\left(\frac{\partial p_2}{\partial y}\right)\right)\widetilde{q_{2h}}\nu_{22} + \left(\frac{\partial p_2}{\partial z} - M_2\left(\frac{\partial p_2}{\partial z}\right)\right)\widetilde{q_{2h}}\nu_{23}\right)ds\right|\right) \\
&\le C\left(\sum_{K\in\mathcal{T}_{1h}} h_K|p_1|_{2,K}|q_{1h}|_{1,K} + \sum_{K\in\mathcal{T}_{2h}} h_K|p_2|_{2,K}|q_{2h}|_{1,K}\right) \\
&\le Ch\left(\sum_{K\in\mathcal{T}_{1h}} |p_1|_{2,K}|\mathbf{q}_h|_{1,K} + \sum_{K\in\mathcal{T}_{2h}} |p_2|_{2,K}|\mathbf{q}_h|_{1,K}\right),
\end{aligned}
\tag{3.16}
$$

where $M_i(\varphi) = \sum_{K\in\mathcal{T}_{ih}}\sum_{E\in\partial K}\frac{1}{\text{meas}(E)}\int_E \varphi ds$ with $i = 1, 2$.

Finally, the error estimate (3.12) follows from (3.5), (3.13) and (3.16). □

**Lemma 3.3** *For* $(q_1, q_2, q_\gamma)$ *and* $(q_{1h}, q_{2h}, q_{\gamma h})$ *defined as in* (2.1) *and* (2.4)*, we have*

$$
|\widetilde{q_{ih}}|_{1,K} \le Ch(|q_1|_{2,h} + |q_2|_{2,h} + \|q_\gamma\|_{2,\Omega_\gamma}), \tag{3.17}
$$

*for* $i = 1, 2$.

***Proof*** Let $\varphi_{ih} = q_{ih} - \Pi_i q_i$ for $i = 1, 2$, then $\widetilde{\varphi_{ih}} = \widetilde{q_{ih}}$. By Lemma 2.3, Theorem 3.1 and (3.3),

$$
\begin{aligned}
|\widetilde{q_{ih}}|_{1,K} &= |\widetilde{\varphi_{ih}}|_{1,K} \le C|\varphi_{ih}|_{1,K} \\
&\le C|q_{ih} - \Pi_i q_i|_{1,K} \\
&\le C|q_{ih} - q_i + q_i - \Pi_i q_i|_{1,K} \\
&\le Ch(|q_1|_{2,h} + |q_2|_{2,h} + \|q_\gamma\|_{2,\Omega_\gamma}).
\end{aligned}
\tag{3.18}
$$

□

The following theorem gives the $L^2$ norm error estimate.

**Theorem 3.2** *Suppose* $\mathbb{K}_1 = k_1\mathbb{I}$, $\mathbb{K}_2 = k_2\mathbb{I}$, $\mathbf{p} = (p_1, p_2, p_\gamma)$ *and* $\mathbf{p}_h = (p_{1h}, p_{2h}, p_{\gamma h})$ *are defined by* (2.1) *and* (2.4)*, respectively. We have*

$$\|\mathbf{p} - \mathbf{p}_h\|_{0,\Omega} \leq Ch^2 \left(|p_1|_{2,h} + |p_2|_{2,h} + \|p_\gamma\|_{2,\Omega_\gamma}\right), \tag{3.19}$$

*where the constant* $C$ *depends on the hydraulic conductivity tensors* $\mathbb{K}_1, \mathbb{K}_2$*, the conduct constant* $\mathbb{K}_{\gamma\tau}$*, the pressures* $p_1, p_2, p_\gamma$ *and the subdivision of mesh grids.*

***Proof*** Following the idea of Aubin–Nitsche method [24,26–28], we let $\mathbf{\Psi} = (\psi_1, \psi_2, \psi_\gamma) \in L^2(\Omega_1) \times L^2(\Omega_2) \times L^2(\Omega_\gamma)$ and consider the following adjoint problem for $\mathbf{\Phi} = (\phi_1, \phi_2, \phi_\gamma) \in H_0^1(\Omega_1) \times H_0^1(\Omega_2) \times H_0^1(\Omega_\gamma)$:

$$\begin{cases} -\mathrm{div}(\mathbb{K}_i \nabla \phi_i) = \psi_i & \text{in } \Omega_i, \quad i = 1, 2, \\ -\mathrm{div}_\tau(K_{\gamma\tau} d \nabla_\tau \phi_\gamma) = \alpha \left( \dfrac{\phi_1 \mid_{\Omega_\gamma} + \phi_2 \mid_{\Omega_\gamma}}{2} - \phi_\gamma \right) + \psi_\gamma & \text{in } \Omega_\gamma, \\ \mathbb{K}_1 \nabla \phi_1 \cdot \mathbf{n}_1 \mid_{\Omega_\gamma} + \mathbb{K}_2 \nabla \phi_2 \cdot \mathbf{n}_2 \mid_{\Omega_\gamma} = \alpha \left( \phi_\gamma - \dfrac{\phi_1 \mid_{\Omega_\gamma} + \phi_2 \mid_{\Omega_\gamma}}{2} \right) & \text{in } \Omega_\gamma, \\ \phi_i = \vartheta_i & \text{on } \Gamma_i, \quad i = 1, 2, \gamma \end{cases} \tag{3.20}$$

with the following regularity estimate

$$\|\phi_1\|_{2,\Omega_1} + \|\phi_2\|_{2,\Omega_2} + \|\phi_\gamma\|_{2,\Omega_\gamma} \leq C(\|\psi_1\|_{0,\Omega_1} + \|\psi_2\|_{0,\Omega_2} + \|\psi_\gamma\|_{0,\Omega_\gamma}). \tag{3.21}$$

By Green's formula, (2.4) and the fact that $p_i, \overline{p_{ih}} \in C^0(\Omega_i)$ with $i = 1, 2$, we have

$$\begin{aligned} (\mathbf{\Psi}, \mathbf{p} - \mathbf{p}_h) = &- \sum_{K \in \mathcal{T}_{1h}} \int_K \mathrm{div}(\mathbb{K}_1 \nabla \phi_1)(p_1 - p_{1h}) dxdydz \\ &- \sum_{K \in \mathcal{T}_{2h}} \int_K \mathrm{div}(\mathbb{K}_2 \nabla \phi_2)(p_2 - p_{2h}) dxdydz \\ &- \sum_{E \in \mathcal{T}_{\gamma h}} \int_E \mathrm{div}_\tau(K_{\gamma\tau} d \nabla_\tau \phi_\gamma)(p_\gamma - p_{\gamma h}) dxdy \\ &+ \alpha \sum_{E \in \mathcal{T}_{\gamma h}} \int_E \left( \phi_\gamma - \frac{\phi_1 \mid_{\Omega_\gamma} + \phi_2 \mid_{\Omega_\gamma}}{2} \right) (p_\gamma - p_{\gamma h}) dxdy \\ = &\, a_h(\mathbf{\Phi}, \mathbf{p} - \mathbf{p}_h) - \sum_{E \in \partial \mathcal{T}_{1h} \setminus \mathcal{T}_{\gamma h}} \int_E \mathbb{K}_1 \nabla \phi_1 \cdot \nu_1 (p_1 - p_{1h}) ds \\ &- \sum_{E \in \partial \mathcal{T}_{2h} \setminus \mathcal{T}_{\gamma h}} \int_E \mathbb{K}_2 \nabla \phi_2 \cdot \nu_2 (p_2 - p_{2h}) ds. \end{aligned} \tag{3.22}$$

Next, we estimate the right-hand side of (3.22).

According to Theorem 2.2, (2.6) and (3.21), we have

$$\begin{aligned} |a_h(\mathbf{\Phi}, \mathbf{p} - \mathbf{p}_h)| &\leq C \|\mathbf{\Phi} - \mathbf{\Pi \Phi}\|_{1,h} \|\mathbf{p} - \mathbf{p}_h\|_{1,h} \\ &\leq Ch(|\phi_1|_{2,\Omega_1} + |\phi_2|_{2,\Omega_2} + \|\phi_\gamma\|_{2,\Omega_\gamma}) \|\mathbf{p} - \mathbf{p}_h\|_{1,h} \\ &\leq Ch^2 \|\mathbf{\Psi}\|_{0,\Omega} (|p_1|_{2,h} + |p_2|_{2,h} + \|p_\gamma\|_{2,\Omega_\gamma}). \end{aligned} \tag{3.23}$$

By combing the fact that $\int_K \nabla \widetilde{p_{ih}} dxdydz = 0$, Green's formula, Lemma 2.3, Lemma 3.2, Theorem 3.1 and (3.21), we have

$$
\begin{aligned}
&\left| \sum_{E\in\partial\mathcal{T}_{1h}\backslash\mathcal{T}_{\gamma h}} \int_E \mathbb{K}_1\nabla\phi_1\cdot\nu_1(p_1-p_{1h})ds + \sum_{E\in\partial\mathcal{T}_{2h}\backslash\mathcal{T}_{\gamma h}} \int_E \mathbb{K}_2\nabla\phi_2\cdot\nu_2(p_2-p_{2h})ds \right| \\
&\le \left| \sum_{K\in\mathcal{T}_{1h}} \int_K \operatorname{div}(\mathbb{K}_1\nabla\phi_1)(p_1-p_{1h})dxdydz - \sum_{K\in\mathcal{T}_{1h}} \int_K \mathbb{K}_1\nabla\phi_1\cdot\nabla(p_1-p_{1h})dxdydz \right| \\
&\quad + \left| \sum_{K\in\mathcal{T}_{2h}} \int_K \operatorname{div}(\mathbb{K}_2\nabla\phi_2)(p_2-p_{2h})dxdydz - \sum_{K\in\mathcal{T}_{2h}} \int_K \mathbb{K}_2\nabla\phi_2\cdot\nabla(p_2-p_{2h})dxdydz \right| \\
&= \left| \sum_{K\in\mathcal{T}_{1h}} \int_K \operatorname{div}(\mathbb{K}_1\nabla\phi_1)\widetilde{p_{1h}}dxdydz - \sum_{K\in\mathcal{T}_{1h}} \int_K (\mathbb{K}_1\nabla\phi_1 - M_1(\mathbb{K}_1\nabla\phi_1))\cdot\nabla\widetilde{p_{1h}}dxdydz \right| \\
&\quad + \left| \sum_{K\in\mathcal{T}_{2h}} \int_K \operatorname{div}(\mathbb{K}_2\nabla\phi_2)\widetilde{p_{2h}}dxdydz - \sum_{K\in\mathcal{T}_{2h}} \int_K (\mathbb{K}_2\nabla\phi_2 - M_2(\mathbb{K}_2\nabla\phi_2))\cdot\nabla\widetilde{p_{2h}}dxdydz \right| \\
&\le C\Bigg( \sum_{K\in\mathcal{T}_{1h}} (|\phi_1|_{2,K}\|\widetilde{p_{1h}}\|_{0,K} + h|\phi_1|_{2,K}|\widetilde{p_{1h}}|_{1,K}) \\
&\quad + \sum_{K\in\mathcal{T}_{2h}} (|\phi_2|_{2,K}\|\widetilde{p_{2h}}\|_{0,K} + h|\phi_2|_{2,K}|\widetilde{p_{2h}}|_{1,K}) \Bigg) \\
&\le Ch^2\Bigg( \sum_{K\in\mathcal{T}_{1h}} |\phi_1|_{2,K}(|p_1|_{2,h} + |p_2|_{2,h} + \|p_\gamma\|_{2,\Omega_\gamma}) \\
&\quad + \sum_{K\in\mathcal{T}_{2h}} |\phi_2|_{2,K}(|p_1|_{2,h} + |p_2|_{2,h} + \|p_\gamma\|_{2,\Omega_\gamma}) \Bigg) \\
&\le Ch^2\|\boldsymbol{\Psi}\|_{0,\Omega}(|p_1|_{2,h} + |p_2|_{2,h} + \|p_\gamma\|_{2,\Omega_\gamma}).
\end{aligned} \tag{3.24}
$$

Finally, in view of (3.22)–(3.24), and

$$
\|\mathbf{p}-\mathbf{p}_h\|_{0,\Omega} = \sup_{\boldsymbol{\Psi}\in L^2(\Omega_1)\times L^2(\Omega_2)\times L^2(\Omega_\gamma)} \frac{(\boldsymbol{\Psi}, \mathbf{p}-\mathbf{p}_h)}{\|\boldsymbol{\Psi}\|_{0,\Omega}}, \tag{3.25}
$$

we arrive at (3.19). □

**Table 1** Errors of Example 1 on uniform cubic mesh

| Mesh | $\|e_p\|_{0,\Omega_p}$ | $\|e_p\|_{1,h}$ | $\|e_\gamma\|_{0,\Omega_\gamma}$ | $\|e_\gamma\|_{1,\Omega_\gamma}$ |
|---|---|---|---|---|
| $6 \times 6 \times 6$ | 2.1357e−01 | 3.6144e−01 | 3.3263e−01 | 5.4536e−01 |
| $8 \times 8 \times 8$ | 1.2738e−01 | 2.5609e−01 | 1.9617e−01 | 4.0681e−01 |
| $16 \times 16 \times 16$ | 3.8688e−02 | 1.2221e−01 | 5.6934e−02 | 2.0523e−01 |
| $32 \times 32 \times 32$ | 1.1687e−02 | 6.2290e−02 | 1.5125e−02 | 1.0168e−01 |
| $64 \times 64 \times 64$ | 3.3517e−03 | 3.0082e−02 | 4.3012e−03 | 5.1756e−02 |
| Rate | 1.7477 | 1.0405 | 1.8403 | 0.9957 |

## 4 Numerical Examples

In this section, we investigate the numerical performance of the proposed numerical scheme for the following model problem

$$\begin{cases} -\mathrm{div}(\mathbb{K}_i \nabla p_i) = g_i & \text{in } \Omega_i, \quad i = 1, 2, \\ -\mathrm{div}_\tau(K_{\gamma\tau} d \nabla_\tau p_\gamma) = \alpha \left( \dfrac{p_1 \,|_{\Omega_\gamma} + p_2 \,|_{\Omega_\gamma}}{2} - p_\gamma \right) + g_\gamma & \text{in } \Omega_\gamma, \\ \mathbb{K}_1 \nabla p_1 \cdot \mathbf{n}_1 \,|_{\Omega_\gamma} + \mathbb{K}_1 \nabla p_2 \cdot \mathbf{n}_2 \,|_{\Omega_\gamma} = \alpha \left( p_\gamma - \dfrac{p_1 \,|_{\Omega_\gamma} + p_2 \,|_{\Omega_\gamma}}{2} \right) & \text{in } \Omega_\gamma, \end{cases} \tag{4.1}$$

with $d = 10^{-3}$.

***Example 1*** Consider the model (4.1) on the domain $\Omega_p = (0, 1) \times (0, 1) \times (-0.5, 0.5)$ and $\Omega_\gamma = (0, 1) \times (0, 1) \times \{z = 0\}$. We use the uniform cubic meshes for this example. The right-hand side functions are determined according to the following analytic solution

$$\begin{cases} p_\gamma = (10{,}001\cos(4\pi y)\sin(2\pi x))/10{,}000 & \text{in } \Omega_\gamma, \\ p_1 = e^{2z}\sin(2\pi x)\cos(4\pi y) & \text{in } (0, 1) \times (0, 1) \times (-1/2, 0] \in \Omega_1, \\ p_2 = e^{-2z}\sin(2\pi x)\cos(4\pi y) & \text{in } (0, 1) \times (0, 1) \times [0, 1/2) \in \Omega_2, \end{cases} \tag{4.2}$$

with $\mathbb{K}_\gamma = 10\mathbb{I}$, $\mathbb{K}_1 = \mathbb{K}_2 = \mathbb{I}$ and $\xi = 1$, $\alpha = 40{,}000$.

Let $(e_p, e_\gamma)$ denote the errors obtained by applying the new nonconforming finite element scheme (2.1) to model problem (4.1). The results are listed in Table 1. The convergence rates are calculated by applying a least-square fitting method to the computational errors with the various mesh sizes.

In order to demonstrate the advantages of the new nonconforming element for solving the Darcy equation in three-dimensional porous media, we compare this approach with the ones using piecewise bilinear $Q_1$ element and Wilson nonconforming finite element. The numerical errors are plotted in Fig. 3. One can observe that the performance of the new element are better than the others with same nodal points and computational costs, due to the fact that the new nonconforming element meets the physical property of the asymptotic model (1.3). The volumetric slice plots of exact solution and numerical solution obtained by our new method are shown in Fig. 4.

***Example 2*** Consider the same domain defined as in Example 1, and use cuboid meshes for this example. Here, we choose the following analytic solution and determine the right-hand

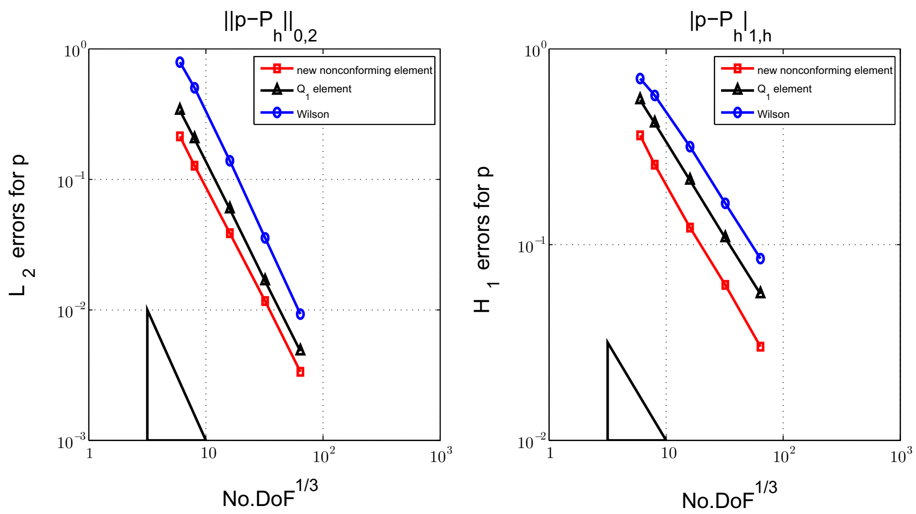


**Fig. 3** Log–log plots of errors of $p_1$ and $p_2$ for Example 1 on uniform cubic grid. Left: $L^2$ norm; right: $H^1$ norm

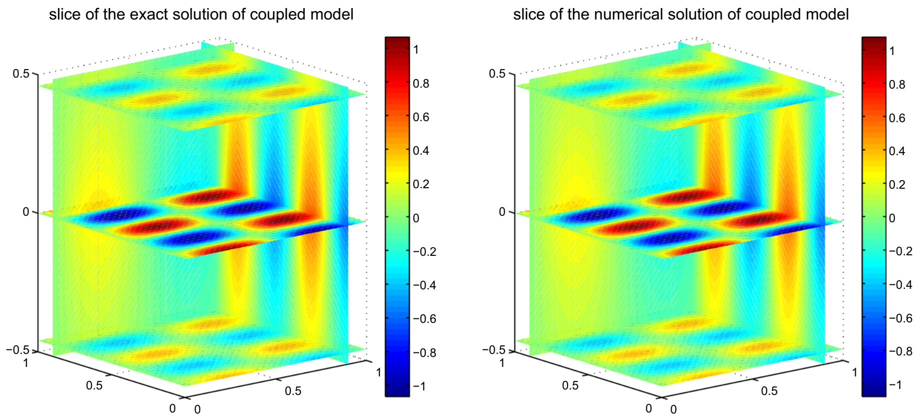


**Fig. 4** Plots of solutions for Example 1 on uniform cubic grid. Left: exact solution $\mathbf{p}$; right: numerical solution $\mathbf{p}_h$

side functions accordingly.

$$\begin{cases} p_\gamma = (11{,}987x^2y^2(x-1)^2(y-1)^2)/12{,}000 & \text{in } \Omega_\gamma, \\ p_1 = (1-10z)(x-x^2)^2(y-y^2)^2 & \text{in } (0,1)\times(0,1)\times(-1/2,0] \in \Omega_1, \\ p_2 = (1+0.1z)^3(x-x^2)^2(y-y^2)^2 & \text{in } (0,1)\times(0,1)\times[0,1/2) \in \Omega_2, \end{cases} \tag{4.3}$$

with $\mathbb{K}_1 = \mathbb{I}$, $\mathbb{K}_2 = 10\mathbb{I}$, $\xi = \frac{2}{3}$, $\alpha = 12{,}000$, $\mathbb{K}_\gamma = \begin{pmatrix} K_{\gamma\tau} & 0 \\ 0 & K_{\gamma n} \end{pmatrix} = \begin{pmatrix} 10 & 0 \\ 0 & 1 \end{pmatrix}$.

The errors obtained by the new nonconforming element are listed in Table 2. One can observe second-order convergence rate for $L^2$ norm and first-order convergence rate for $H^1$ norm, which are consistent with the theoretical results in Theorems 3.1 and 3.2. We also compare our new nonconforming element with $Q_1$ element and Wilson element for this

**Table 2** Errors of Example 2 on cuboid mesh

| Mesh | $\|e_p\|_{0,\Omega_p}$ | $\|e_p\|_{1,h}$ | $\|e_\gamma\|_{0,\Omega_\gamma}$ | $\|e_\gamma\|_{1,\Omega_\gamma}$ |
|---|---|---|---|---|
| $4\times4\times4$ | 8.8490e−02 | 2.5144e−01 | 1.4521e−01 | 4.0413e−01 |
| $8\times8\times8$ | 2.0738e−02 | 1.2566e−01 | 4.1432e−02 | 2.2589e−01 |
| $16\times16\times16$ | 4.9842e−03 | 6.2262e−02 | 1.0634e−02 | 1.1574e−01 |
| $32\times32\times32$ | 1.2271e−03 | 3.1041e−02 | 2.6727e−03 | 5.8321e−02 |
| $64\times64\times64$ | 3.0012e−04 | 1.5442e−02 | 6.7701e−04 | 2.9462e−02 |
| Rate | 2.0487 | 1.0068 | 1.9444 | 0.9509 |

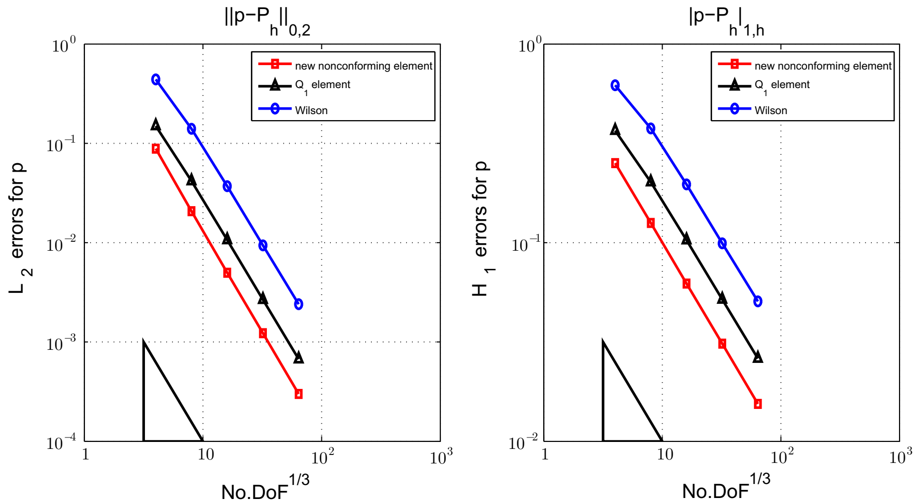


**Fig. 5** Log–log plots of errors of $p_1$ and $p_2$ for Example 2 on cuboid grid. Left: $L^2$ norm; right: $H^1$ norm

example, and report the errors in Fig. 5. The exact solution and numerical solution obtained by the new nonconforming method are depicted in Fig. 6.

***Example 3*** Consider the model problem (4.1) on a domain with refined meshes near the fracture. The analytic solution is chosen as

$$\begin{cases} p_\gamma = 40{,}001\sin(2\pi x)\sin(\pi y)/40{,}000 & \text{in } \Omega_\gamma, \\ p_1 = \sin(2\pi x)\sin(\pi y) & \text{in } \Omega_1, \\ p_2 = (1-z)\sin(2\pi x)\sin(\pi y) & \text{in } \Omega_2, \end{cases} \tag{4.4}$$

with $\mathbb{K}_\gamma = 10\mathbb{I}$, $\mathbb{K}_1 = \mathbb{K}_2 = \mathbb{I}$ and $\xi = 1$, $\alpha = 40{,}000$. The right-hand side functions are determined accordingly.

The errors are reported in Table 3 (Fig. 7). The numerical solution $\mathbf{p}_h$ and exact solution $\mathbf{p}$ are depicted in Fig. 8, where refined meshes are employed near the fracture to capture the more rapid change of flow pressure. Moreover, as shown in Fig. 7, the errors obtained by new nonconforming element is evidently smaller than that of $Q_1$ element and Wilson element. In particular, the new method attains higher order convergence rates in $H^1$ norm.

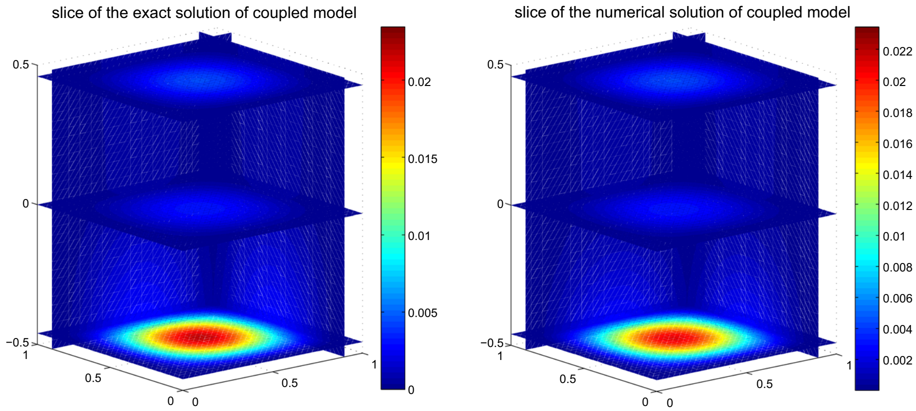


**Fig. 6** Plots of solutions for Example 2 on cuboid grid. Left: exact solution $\mathbf{p}$; right: numerical solution $\mathbf{p}_h$

**Table 3** Errors of Example 3 with mesh refined near the fracture

| Mesh | $\Vert e_p \Vert_{0,\Omega_p}$ | $\vert e_p \vert_{1,h}$ | $\Vert e_\gamma \Vert_{0,\Omega_\gamma}$ | $\Vert e_\gamma \Vert_{1,\Omega_\gamma}$ |
|---|---|---|---|---|
| $4 \times 4 \times 4$ | 1.9326e−02 | 5.5955e−02 | 4.8605e−2 | 2.2462e−01 |
| $8 \times 8 \times 8$ | 4.1087e−03 | 1.4029e−02 | 1.2713e−2 | 1.1301e−01 |
| $16 \times 16 \times 16$ | 9.7356e−04 | 3.5098e−03 | 3.2798e−3 | 5.6620e−02 |
| $32 \times 32 \times 32$ | 2.2201e−04 | 8.9113e−04 | 8.3106e−4 | 2.8298e−02 |
| $64 \times 64 \times 64$ | 5.4878e−05 | 2.2829e−04 | 2.2872e−4 | 1.3637e−02 |
| Rate | 2.1130 | 1.9851 | 1.9398 | 1.0081 |

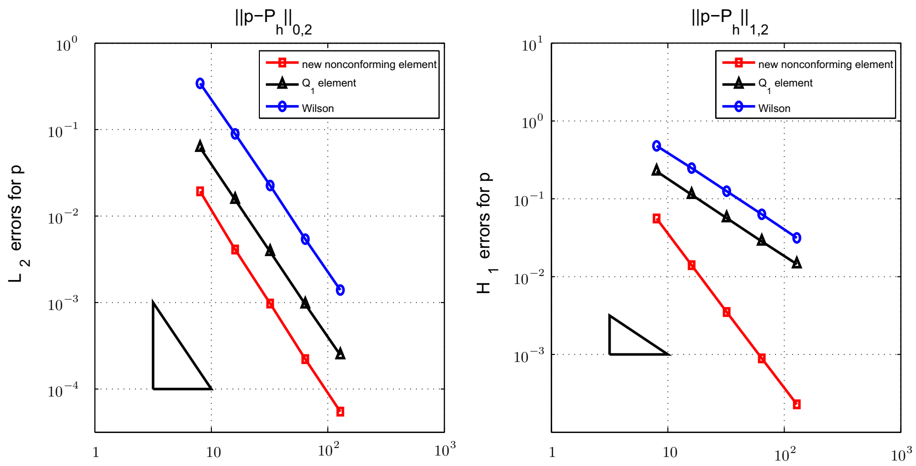


**Fig. 7** Log–log plots of errors of $p_1$ and $p_2$ for Example 3 with mesh refinement near the fracture. Left: $L^2$ norm; right: $H^1$ norm

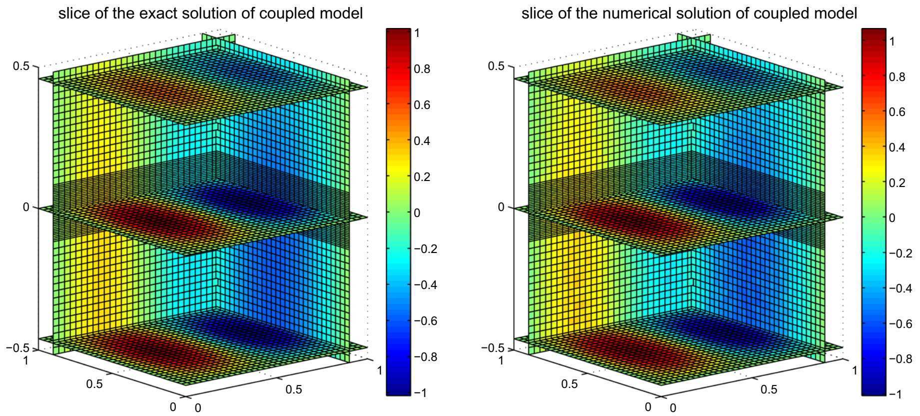


**Fig. 8** Plots of solutions for Example 3 with mesh refinement near the fracture. Left: exact solution $\mathbf{p}$; right: numerical solution $\mathbf{p}_h$

**Table 4** Errors of Example 4 on uniform mesh

| Mesh | $\|E_p\|_{0,\Omega_p}$ | $\|E_p\|_{1,h}$ | $\|E_\gamma\|_{0,\Omega_\gamma}$ | $\|E_\gamma\|_{1,\Omega_\gamma}$ |
|---|---|---|---|---|
| $8\times8\times8$ | – | – | – | – |
| $16\times16\times16$ | 3.7213 | 1.8622 | 3.8479 | 1.8759 |
| $32\times32\times32$ | 3.8766 | 1.8730 | 3.8731 | 1.8954 |
| $64\times64\times64$ | 3.8972 | 1.9058 | 3.9016 | 1.9019 |
| Rate | 1.9158 | 0.9402 | 1.9371 | 0.9455 |

***Example 4*** In this example, we use the numerical scheme (2.1) and uniform cubic mesh to solve the problem with following source terms:

$$\begin{cases} g_\gamma = 1000\sin(\pi x)\sin(2\pi y), \\ g_1 = 0, \\ g_2 = 0, \\ P|_{\Gamma_\gamma} = 0, \\ P|_{z=0.5} = 0, \\ P|_{z=-0.5} = 0, \\ P|_{x=0\cup x=1\cup y=0\cup y=1} = 0, \end{cases} \tag{4.5}$$

where $\mathbb{K}_\gamma = 2.5\mathbb{I}$, $\mathbb{K}_1 = \mathbb{K}_2 = \mathbb{I}$ and $\xi = 1$, $\alpha = 10{,}000$.

Since the analytic solutions are not available in this case, we define the following errors

$$E_i = \frac{p_{i,h} - p_{i,h/2}}{p_{i,h/2} - p_{i,h/4}}, (i = 1, 2), \quad E_\gamma = \frac{p_{\gamma,h} - p_{\gamma,h/2}}{p_{\gamma,h/2} - p_{\gamma,h/4}},$$

and the norm $\|E_p\| = \|E_1\| + \|E_2\|$. In order to test the accuracy using errors between consecutive levels, the bilinear interpolation method is used interpolate function values from coarse grids to fine grids. One can observe from Table 4 that the errors are second-order accurate in $L^2$ norm and first-order in $H^1$ norm.

The numerical solutions in fracture $\Omega_\gamma$ and whole domain are plotted in Fig. 9. According to the boundary condition in (4.5), the values of pressures vary faster along $z$-direction than the other two directions. The pressures on the fracture hyperplane show the sine and cosine

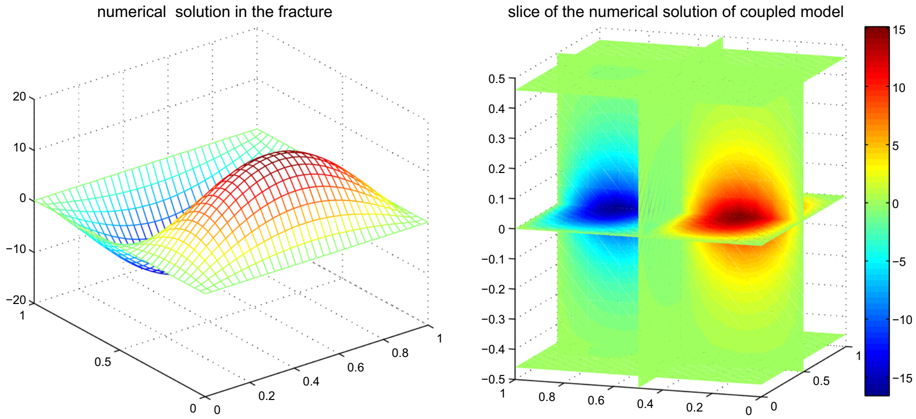


**Fig. 9** Plots of numerical solution for Example 4 on uniform cubic grid. Left: $p_{\gamma h}$; right: $\mathbf{p}_h$

patterns with the source term $g_\gamma$. As shown in Fig. 9, the behavior of numerical pressure can effectively capture the desired physical feature.

***Example 5*** In this example, we extend the idea of constructing new nonconforming element to an inclined fracture. For example, one element is based on the combination of $Q_1$ element and Quasi-Wilson element. The basis functions can chosen as follows

$$\hat{\mathbb{P}} = Q_1(\hat{K}) \bigoplus span\left\{\frac{(1-x^2)(1-y^2)(1-5x^2)(1-5y^2)}{144}\right\},$$

with

$$\widehat{\sum} = \left\{\hat{q}(\hat{v}_i), i = 1, \ldots, 8;\ \frac{\partial^4 \hat{q}}{\partial \hat{x}^2 \partial \hat{y}^2}(0,0,0)\right\}.$$

The inclined fracture domain is defined as $\Omega_\gamma := \{z = x/4, x \in [0,1], y \in [0,1]\}$. We divide each edge along $z$-direction into equal-length segments and obtain the meshes with $n \times n \times n$ hexahedron elements for porous media $\Omega_p$. Consider the problem with the following exact solution

$$\begin{cases} p_\gamma = \left(\frac{\sqrt{17}}{3.2\times 10^4} + 1 - \frac{x}{4}\right)\sin(2\pi x)\sin(2\pi y) & \text{in } \Omega_\gamma, \\ p_1 = \left(1 - \frac{x}{4}\right)\sin(2\pi y)\sin(2\pi x) & \text{in } \Omega_1, \\ p_2 = (1-z)\sin(2\pi y)\sin(2\pi x) & \text{in } \Omega_2, \end{cases} \tag{4.6}$$

where $\mathbb{K}_\gamma = 2\mathbb{I}, \mathbb{K}_1 = \mathbb{K}_2 = \mathbb{I}$ and $\xi = 1, \alpha = 8000$. The right-hand side functions are determined accordingly. The errors of new nonconforming element are reported in Table 5.

In order to show the advantages of new element, we compare it with $Q_1$ element and quasi-Wilson element. It can be seen from Fig. 10 that the errors obtained by the new element is the smallest one. Moreover, from the Fig. 11 we can see that the new nonconforming method is effective in approximating solutions of the asymptotic model with inclined fracture.

## 5 Conclusion

In this work we introduced and analyzed a numerical method coupled a new nonconforming element with a conforming element for solving the asymptotic model problem (1.3). The

**Table 5** Errors of Example 5 with inclined fracture

| Mesh | $\|e_p\|_{0,\Omega_p}$ | $\|e_p\|_{1,h}$ | $\|e_\gamma\|_{0,\Omega_\gamma}$ | $\|e_\gamma\|_{1,\Omega_\gamma}$ |
|---|---|---|---|---|
| $4\times4\times4$ | 2.1455e−01 | 4.5261e−01 | 2.6720e−01 | 5.2125e−01 |
| $8\times8\times8$ | 5.5276e−02 | 2.3989e−01 | 6.8576e−02 | 2.7102e−01 |
| $16\times16\times16$ | 1.4953e−02 | 1.2212e−01 | 1.8462e−02 | 1.471e−01 |
| $32\times32\times32$ | 3.6267e−03 | 6.4017e−02 | 4.9210e−03 | 7.6667e−02 |
| $64\times64\times64$ | 9.1759e−04 | 3.2733e−02 | 1.9035e−03 | 4.1869e−02 |
| Rate | 1.9668 | 0.9485 | 1.8067 | 0.9098 |

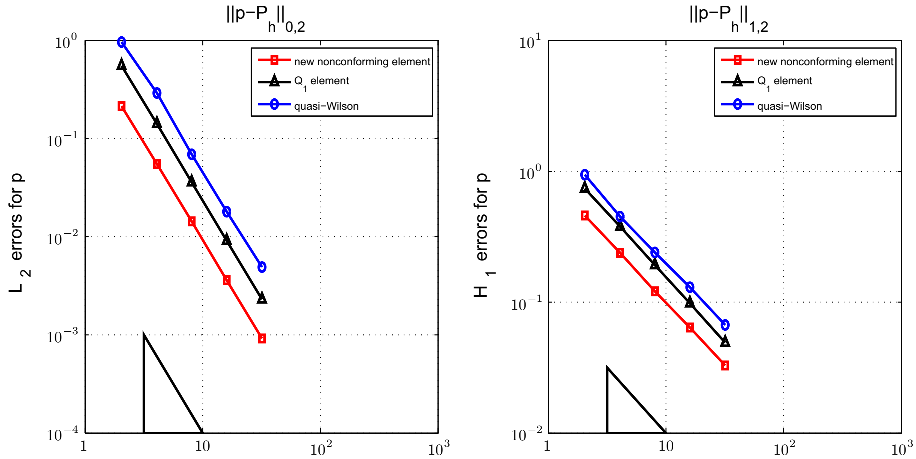


**Fig. 10** Log–log plots of errors of $p_1$ and $p_2$ for Example 5 with inclined fracture. Left: $L^2$ norm; right: $H^1$ norm

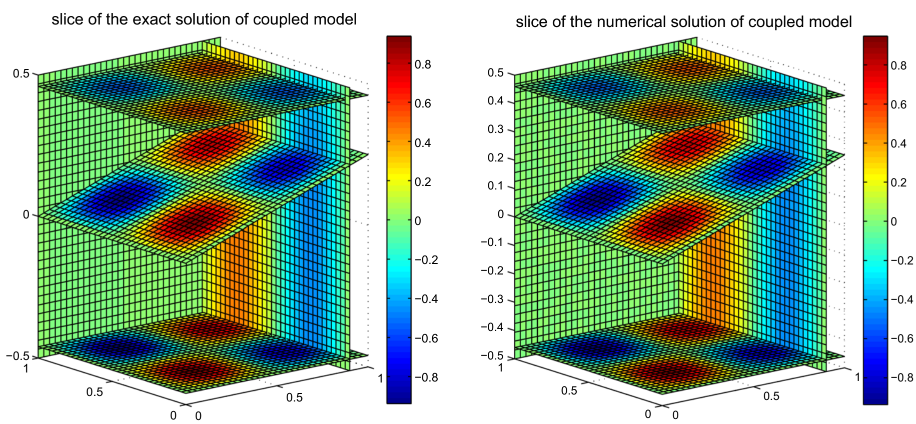


**Fig. 11** Plots of solutions for Example 5 with inclined fracture. Left: exact solution $\mathbf{p}$; right: numerical solution $\mathbf{p}_h$

new element is anisotropic and continuous along the direction parallel to the fracture and discontinuous along the direction perpendicular to the fracture. It is an appropriate scheme for solving the fractured aquifer model since it coincides with the physical feature of the solution of practical problem. On the same mesh grids with the same amount of computational cost, the errors obtained by the new nonconforming element are smaller than those of $Q_1$ element and Wilson element. For other domains with more complicated geometry, one can deduce the shape functions for new elements by using similar idea introduced in this paper. This is also our future work.

## References

1. Bauer, S., Liedl, R., Sauter, M.: Modeling of karst aquifer genesis: influence of exchange flow. Water Resour. Res. **39**(10), 371–375 (2003)
2. Bauer, S., Liedl, R., Sauter, M., Stauffer, F., Kinzelbach, W., Kovar, K., Hoehn, E.: Modelling of karst development considering conduit-matrix exchange flow. In: Calibration and Reliability in Groundwater Modelling: Coping with Uncertainty. Proceedings of the ModelCARE'99 Conference Held in Zurich, Switzerland, 20–23 Sept 1999 (2000)
3. Birk, S., Liedl, R., Sauter, M., Teutsch, G.: Hydraulic boundary conditions as a controlling factor in karst genesis: a numerical modeling study on artesian conduit development in gypsum. Water Resour. Res. **39**(1), SBH 2-1–SBH 2-14 (2003)
4. Espinosa-Paredes, G., Morales-Zárate, E., Vázquez-Rodríguez, A.: Analytical analysis for mass transfer in a fractured porous medium. Pet. Sci. Technol. **31**(19), 2004–2012 (2013)
5. Cao, Y., Fei, H., Wang, X.: Analysis and finite element approximation of a coupled, continuum pipe-flow/Darcy model for flow in porous media with embedded conduits. Numer. Methods Partial Differ. Equ. **27**(5), 1242–1252 (2011)
6. Chen, N., Gunzburger, M., Hu, B., Wang, X., Woodruff, C.: Calibrating the exchange coefficient in the modified coupled continuum pipe-flow model for flows in karst aquifers. J. Hydrol. **414–415**(2), 294–301 (2012)
7. Liu, W., Zhao, Q., Li, X., Li, J.: Anisotropic wilson element with conforming finite element approximation for a coupled continuum pipe-flow/Darcy model in karst aquifers. Math. Methods Appl. Sci. **38**(17), 4024–4037 (2015)
8. Liu, W., Kang, Z., Rui, H.: Finite volume element approximation of the coupled continuum pipe-flow/Darcy model for flows in karst aquifers. Numer. Methods Partial Differ. Equ. **30**(2), 376–392 (2014)
9. Liu, W., Cui, J., Xin, J.: A block-centered finite difference method for an unsteady asymptotic coupled model in fractured media aquifer system. J. Comput. Appl. Math. **337**, 319–340 (2018)
10. Wang, X.: On the coupled continuum pipe flow model (CCPF) for flows in karst aquifer. Discrete Contin. Dyn. Syst. Ser. B **13**(2), 489–501 (2009)
11. Chen, Z., An, K., Liu, Y., Chen, W.: Adjoint method for an inverse problem of CCPF model. Chin. Ann. Math. **3**(3), 337–354 (2014)
12. Liedl, R., Sauter, M., Hückinghaus, D., Clemens, T., Teutsch, G.: Simulation of the development of karst aquifers using a coupled continuum pipe flow model. Water Resour. Res. **39**(3), 597–676 (2003)
13. Wu, X., Kügler, P., Lu, S.: Identification of the exchange coefficient from indirect data for a coupled continuum pipe-flow model. Chin. Ann. Math. **35**(3), 483–500 (2014)
14. Martin, V., Jaffré, J., Roberts, J.E.: Modeling fractures and barriers as interfaces for flow in porous media. SIAM J. Sci. Comput. **26**(5), 1667–1691 (2005)
15. Hoang, T.-T.-P., Japhet, C., Kern, M., Roberts, J.E.: Space-time domain decomposition for reduced fracture models in mixed formulation. SIAM J. Numer. Anal. **54**(1), 288–316 (2016)
16. Loper, D.E.: An analytic benchmark test for karst-aquifer flow. Geophys. Astrophys. Fluid Dyn. **107**(5), 587–602 (2013)
17. Yao, B., Wei, J., Wang, D., Ma, D., Chen, Z.: Numerical study on seepage property of karst collapse columns under particle migration. CMES Comput. Model. Eng. Sci. **91**(2), 81–100 (2013)
18. Lesinigo, M., DAngelo, C., Quarteroni, A.: A multiscale Darcy–Brinkman model for fluid flow in fractured porous media. Numer. Math. **117**(4), 717–752 (2011)
19. Angot, P., Boyer, F., Hubert, F.: Asymptotic and numerical modelling of flows in fractured porous media. ESAIM Math. Model. Numer. Anal. **43**(2), 239–275 (2009)

20. Frih, N., Martin, V., Roberts, J.E., Saâda, A.: Modeling fractures as interfaces with nonmatching grids. Comput. Geosci. **16**(4), 1043–1060 (2012)
21. Tunc, X., Faille, I., Gallouët, T., Cacas, M.C., Havé, P.: A model for conductive faults with non-matching grids. Comput. Geosci. **16**(2), 277–296 (2012)
22. Morales, F., Showalter, R.E.: The narrow fracture approximation by channeled flow. J. Math. Anal. Appl. **365**(1), 320–331 (2010)
23. Shi, D., Chen, S.: A class of nonconforming arbitrary quadrilateral elements. Numer. Math. A J. Chin. Univ. **2**, 231–238 (1996)
24. Shi, Z.C., Chen, S.C.: Analysis of a nine degree plate bending element of Shecht. Chin. J. Numer. Math. Appl. **4**, 73–79 (1989)
25. Shi, Z.C., Jiang, B., Xue, W.: A new superconvergence property of Wilson nonconforming finite element. Numer. Math. **78**(2), 259–268 (1997)
26. Wilson, E.L., Taylor, R.L., Doherty, W.P., Ghaboussi, J.: Incompatible Displacement Models. Numerical and Computer Methods in Structural Mechanics, pp. 43–57. Academic Press, New York (1973)
27. Ciarlet, P.G., Lions, J.L.: Handbook of Numerical Analysis. Gulf Professional Publishing (Distributors for the United States), Amsterdam (1990)
28. Shi, Z.C.: A convergence condition for the quadrilateral Wilson element. Numer. Math. **44**(3), 349–361 (1984)